Journal of Fluids and Structures (2002) **16**(1), 31–51
doi:10.1006/jfls.2001.0402, available online at http://www.idealibrary.com on IDEAL®

VIBRATIONS OF CIRCULAR CYLINDRICAL SHELLS WITH NONUNIFORM CONSTRAINTS, ELASTIC BED AND ADDED MASS. PART II: SHELLS CONTAINING OR IMMERSED IN AXIAL FLOW

M. Amabili and R. Garziera

Dipartimento di Ingegneria Industriale, Università di Parma, Parco Area delle Scienze 181/A Parma, I–43100 Italy

(Received 11 May 2000, and in final form 12 February 2001)

The model introduced in Part I of the present study is extended to take into account a flowing fluid, a mean radial pressure and initial pre-stress in circular cylindrical shells. The axial flow can be external, internal or annular and is described by the potential theory for inviscid and incompressible fluid. The computer program DIVA has been developed. It takes into account all the following complicating effects on the vibrations of circular cylindrical shells: (i) nonuniform boundary conditions around the shell edges including elastic boundary conditions; (ii) fluid–structure interaction including both flowing and quiescent fluids; (iii) internal, external and annular fluids; (iv) effect of a mean radial pressure and initial pre-stress; (v) elastic bed of partial extension in circumferential and longitudinal directions; (vi) intermediate constraints; (vii) added masses. It can be considered the most complete computer program specifically dedicated to dynamics of circular cylindrical shells. The Flügge theory of shells is used to describe the shell deformations. The system has been proved to be conservative for any combination of boundary conditions with restrained displacement at the shell ends. Numerical results show that shells clamped at the upstream end and simply supported at the downstream end have a larger critical velocity than simply supported shells, solving the paradox of Horáček and Zolotarev.

1. INTRODUCTION

Shells containing or immersed in flowing fluids are widely used in engineering applications, where they are subjected to excitations of different kinds, including flow excitations. Usually, these shells are made as thin as possible for weight and cost economy; therefore, their response to such excitations is of great interest.

All previous studies on the dynamics of shells containing or immersed in axial flow assumed uniform boundary conditions around the edges. One of the first modern studies on vibrations of circular cylindrical shells containing flowing fluid is due to Niordson (1953). Païdoussis & Denise (1972) considered both clamped and cantilevered shells subjected to axial flow and used a travelling wave-type solution by satisfying the pertinent boundary conditions, along with a separation of variables method to solve the boundary value problem for the fluid–structure interaction. Weaver & Unny (1973), on the other hand, investigated the stability of simply supported shells by means of the Fourier transform method to solve the fluid–structure interaction. Matsuzaki & Fung (1977) included the effect of viscous structural damping and Mizoguchi & Komori (1978) considered a compressible flow. Horáček & Zolotarev (1984) studied the effect of different boundary

0889–9746/02/010031 + 21 $35.00/0

conditions at the shell ends. In particular, they found the surprising result that vibrations of shells conveying flow, simply supported at the upstream end and clamped at the downstream end, are not conservative; moreover, if the boundary conditions are reversed, the shell is unstable for an arbitrarily small fluid velocity. Horáček & Zolotarev (1991) also studied the acoustic–structural coupling of vibrating shells with or in flow. Selmane & Lakis (1997*a*) investigated free vibrations of open and closed circular shells with fluid flow by using a hybrid, finite element method. In these papers, the shell stability as well as the linear dependence of the natural frequencies of the system on the flow velocity have been investigated.

In a subsequent study, Selmane & Lakis (1997*b*) considered the nonlinear vibrations of open and closed circular cylindrical shells with fluid flow by using a hybrid, finite element method and the nonlinear Sanders-Koiter shell theory. Amabili *et al.* (1999, 2000) performed a complete study of the nonlinear stability and forced response of simply supported circular cylindrical shells with flow by using Donnell's nonlinear shallow-shell theory. In particular, they have shown for the first time that the stability of a shell conveying fluid predicted by linear theory can be largely nonconservative and that the stability limit must be calculated by using a nonlinear shell theory.

Vibrations of circular cylindrical shells in unbounded and annular flow have also been deeply investigated. Dowell & Widnall (1966) obtained the aerodynamic forces on an oscillating cylindrical shell in potential, unbounded axial flow by using the Fourier transform method. Païdoussis *et al.* (1984, 1991, 1992) studied coaxial cylindrical shells in annular flow, and for both internal and annular flows the analysis was further extended to deal with a viscous flow (Païdoussis *et al.* 1985). Although viscous effects can be extremely important for annular flows, it was shown that for internal flow they are much less so, which is of particular importance in the present study where the flow is assumed to be inviscid. Other studies on shells in viscous annular flow are due to El Chebair *et al.* (1990) and Nguyen *et al.* (1994). Additional results for inviscid annular flow were obtained by Horáček (1993). Experimental results are given by El Chebair *et al.* (1989) and Nguyen *et al.* (1993). Shells in supersonic flow are not considered in this brief review. No studies are available for circular cylindrical shells with nonuniform boundary conditions around the edge coupled to fluid flow.

In the present study, the model introduced in Part I (Amabili & Garziera 2000) is extended to take into account a flowing fluid, different constraints at the shell edges, a mean radial pressure and initial pre-stress in the shell. The axial flow can be external, internal or annular and is described by the potential theory for inviscid and incompressible fluid. The computer program DIVA has been developed. It takes into account all the following complicating effects on the vibrations of circular cylindrical shells: (i) nonuniform boundary conditions around the shell edges including elastic boundary conditions; (ii) fluid–structure interaction including both flowing and quiescent fluids; (iii) internal, external and annular fluids; (iv) effect of a mean radial pressure and initial pre-stress; (v) elastic bed of partial extent in the circumferential and longitudinal directions; (vi) intermediate constraints; (vii) added masses. It can be considered the most complete computer program specifically dedicated to the dynamics of circular cylindrical shells. The Flügge theory of shells is used to describe the shell deformations. The system has been proved to be conservative for any combination of boundary conditions with restrained displacement at the shell ends.

Thus, the present study solves the paradox obtained by Horáček & Zolotarev (1984), i.e., that shells clamped at the upstream end and simply supported at the downstream end are unstable for an arbitrarily small fluid velocity. In particular, it has been shown that these shells have a larger critical velocity than simply supported shells, as expected. The paradox of Horáček and Zolotarev is probably due to some kind of numerical error in the

eigenvalues evaluation.† For this reason, the program developed here, although optimized for speed, has a very high numerical accuracy.

2. SHELL–FLOW INTERACTION

A cylindrical coordinate system (x, r, θ) is introduced, with the origin at one shell end. The displacement of the shell mean surface is denoted by u, v, w in axial, circumferential and radial directions, respectively (see Figure 1). The shell has radius R, length L and thickness h. The fluid–structure interaction is described by linear potential flow theory. The shell is considered either immersed in annular fluid flow, confined by an internal or external rigid cylinder of radius R_1, or conveying incompressible flow. The case of an unbounded external fluid domain in the radial direction is obtained as a limiting case of the annular flow for $R_1 \to \infty$. The cases with $R_1 < R$ (internal annular flow) and $R_1 \to 0$ (internal flow) are also described by the present model. The fluid is assumed to be inviscid, and the flow to be isentropic and irrotational. Actually, for narrow annular gaps between the shell and the external rigid cylinder, the effects of viscous forces on stability can be significant, as found by Païdoussis *et al.* (1985, 1991). The irrotationality property is the condition for the existence of a scalar potential function Ψ from which the velocity may be written as

$$\mathbf{v} = \nabla\Psi. \tag{1}$$

The potential Ψ consists of two components: one due to the mean flow associated with the undisturbed flow velocity U in the axial direction, and the unsteady perturbation potential Φ associated with shell motion. Thus,

$$\Psi = Ux + \Phi. \tag{2}$$

The potential of the perturbation velocity satisfies the Laplace equation

$$\nabla^2\Phi = \frac{\partial^2\Phi}{\partial x^2} + \frac{\partial^2\Phi}{\partial r^2} + \frac{1}{r}\frac{\partial\Phi}{\partial r} + \frac{1}{r^2}\frac{\partial^2\Phi}{\partial\theta^2} = 0. \tag{3}$$

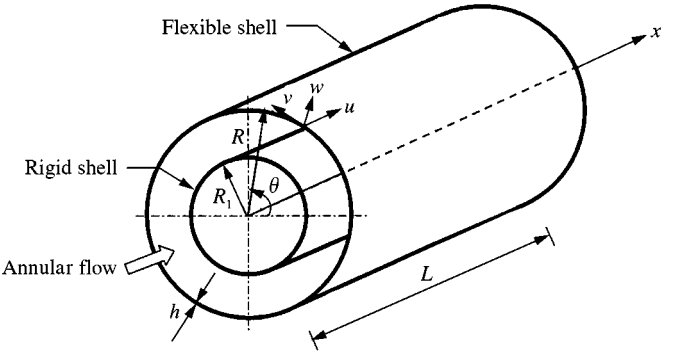

Figure 1. Schematic of the shell with an annular flow. The coordinate system and shell displacements are given.

†The same conclusion has been reached, in a different manner, by Misra *et al.* (2001) and Wong (2000).

The perturbed pressure P may be related to the velocity potential by Bernoulli's equation for unsteady fluid flow,

$$\frac{\partial \Phi}{\partial t} + \tfrac{1}{2} V^2 + \frac{P}{\rho_F} = \frac{P_S}{\rho_F}, \tag{4}$$

where $V^2 = \nabla\Psi \cdot \nabla\Psi$, P_S is the stagnation pressure and ρ_F is the fluid mass density. The pressure P in the fluid domain can be written as

$$P = \bar{P} + p, \tag{5}$$

where $\bar{P}$ is the mean pressure and p is the perturbation pressure, assumed positive outwards as w. For small perturbations, $V^2 \cong U^2 + 2U(\partial\Phi/\partial x)$, and equation (5) gives the stagnation pressure $P_S = \bar{P} + \frac{1}{2}\rho_F U^2$, so that it is fixed for an assumed mean flow velocity. Then, equation (5) gives the following expression for the perturbation pressure:

$$p = -\rho_F \left(\frac{\partial \Phi}{\partial t} + U \frac{\partial \Phi}{\partial x} \right). \tag{6}$$

2.1. Potential of the Perturbation Velocity

The fluid domain is assumed to be an annular cylinder of infinite extent, delimited at $r = R$ by a periodically supported shell of infinite length, and at $r = R_1$ by a rigid cylinder, so that it is possible to employ the method of separation of variables to obtain the velocity potential. Here the mathematical trick is to consider the function w and the fluid domain defined for any $x \in (-\infty, \infty)$. This means that w is a periodic function with main period $2L$, and the same is verified for the velocity potential and the perturbation pressure. This type of solution was initially introduced by Niordson (1953) and then used by Païdoussis & Denise (1972) for shells with incompressible flow, either internal or external. The physical interpretation of this solution is that the shell studied is inserted in an infinitely long pipe periodically supported, where the distance between two consecutive supports is the length L of the shell. Only antisymmetric modes with respect to these supports ($x = 0$, L) are considered because they are those with the lowest frequencies.

Similar to Part I of the present study (Amabili & Garziera 2000), the symmetric modes (in a cross-section) with respect to $\theta = 0$ are expanded as

$$\begin{Bmatrix} u \\ v \\ w \end{Bmatrix}_S = \sum_{n=0}^{\infty} \sum_{m=1}^{\infty} \sum_{j=1}^{3} a_{nmj} \begin{Bmatrix} A_{nmj} \cos(n\theta) \cos(m\pi x/L) \\ B_{nmj} \sin(n\theta) \sin(m\pi x/L) \\ \cos(n\theta) \sin(m\pi x/L) \end{Bmatrix} e^{\Lambda t}, \tag{7}$$

where a_{nmj} are the unknown coefficients involved in the mode expansion, A_{nmj} and B_{nmj} are the mode shape coefficients, and n, m and j indicate the number of circumferential waves, the number of axial half-waves and the mode number, respectively. In equation (7), the imaginary part of Λ is the circular frequency of oscillation of the shell and its real part gives an exponential growth or decay, and t is the time. The antisymmetric modes with respect to $\theta = 0$ are expanded as

$$\begin{Bmatrix} u \\ v \\ w \end{Bmatrix}_A = \sum_{n=1}^{\infty} \sum_{m=1}^{\infty} \sum_{j=1}^{3} b_{nmj} \begin{Bmatrix} A_{nmj} \sin(n\theta) \cos(m\pi x/L) \\ B_{nmj} \cos(n\theta) \sin(m\pi x/L) \\ \sin(n\theta) \sin(m\pi x/L) \end{Bmatrix} e^{\Lambda t}, \tag{8}$$

If there is no cavitation at the fluid–shell interface, the boundary condition expressing the contact between the shell wall and the flow is

$$\left(\frac{\partial \Phi}{\partial r}\right)_{r=R} = \left(\frac{\partial w}{\partial t} + U\,\frac{\partial w}{\partial x}\right). \tag{9}$$

Similarly, at the fluid/rigid-cylinder interface

$$\left(\frac{\partial \Phi}{\partial r}\right)_{r=R_1} = 0. \tag{10}$$

Boundary condition (10) excludes the dynamic interaction between the shell being studied and the external cylinder. In order to investigate the dynamic interaction between two flexible shells, equation (10) must be replaced with an expression of the type of equation (9).

The radial shell displacement w has the generic form $w = A(t)\sin(m\pi x/L)\cos(n\theta)$, as shown by equations (7) and (8). By using the method of separation of variables, Φ has the form

$$\Phi(x, r, \theta, t) = \psi(r)\cos(n\theta)\,\mathrm{e}^{\mathrm{i}\alpha x}\mathrm{e}^{\Lambda t}, \tag{11}$$

where $\alpha = m\pi/L$ is a function of m, and i is the imaginary unit. Substituting equation (11) into equation (3), it is found that

$$\psi(r) = C_1\,\mathrm{I}_n(m\pi r/L) + C_2\,\mathrm{K}_n(m\pi r/L), \tag{12}$$

where C_1 and C_2 are appropriate coefficients. In equation (12), I_n and K_n are the modified Bessel functions of order n of the first and the second kind, respectively. Equations (9) and (10) are satisfied by having Φ of the form

$$\Phi = \frac{\mathrm{K}_n'(\alpha R_1)\,\mathrm{I}_n(\alpha r) - \mathrm{I}_n'(\alpha R_1)\,\mathrm{K}_n(\alpha r)}{\alpha[\mathrm{K}_n'(\alpha R_1)\,\mathrm{I}_n'(\alpha R) - \mathrm{I}_n'(\alpha R_1)\,\mathrm{K}_n'(\alpha R)]}\left(\frac{\partial w}{\partial t} + U\,\frac{\partial w}{\partial x}\right). \tag{13}$$

In order to simplify this notation, the ratio F_{nm} is introduced,

$$F_{nm}(r) = \frac{\mathrm{K}_n'(\alpha R_1)\,\mathrm{I}_n(\alpha r) - \mathrm{I}_n'(\alpha R_1)\,\mathrm{K}_n(\alpha r)}{\mathrm{K}_n'(\alpha R_1)\,\mathrm{I}_n'(\alpha r) - \mathrm{I}_n'(\alpha R_1)\,\mathrm{K}_n'(\alpha r)}. \tag{14}$$

In particular, for symmetric modes as given in equation (7), Φ takes the following form:

$$\Phi = \sum_{n=0}^{\infty}\sum_{m=1}^{\infty}\sum_{j=1}^{3} a_{nmj}\cos(n\theta)\,(L/(m\pi))\,F_{nm}(r)\,\mathrm{e}^{\Lambda t}[\Lambda\sin(m\pi x/L) + U(m\pi/L)\cos(m\,\pi x/L)]. \tag{15}$$

The expression of Φ for antisymmetric modes is immediately obtained from equation (15). For flow inside the shell ($R_1 \to 0$), equation (14) simplifies to

$$F_{nm}(r) = \frac{\mathrm{I}_n(m\pi r/L)}{\mathrm{I}_n'(m\pi R/L)}. \tag{16}$$

2.2. Energy Associated with the Perturbation Potential

Only the effect of the mean flow potential does not give any time-varying contribution in the evaluation of the flow energy, as shown in Appendix A. The energy E_F associated with the perturbation potential, by using the Green theorem, is given by

$$E_F = \mp\frac{1}{2}\rho_F\int_0^{2\pi}\int_0^{L}\left(\Phi\,\frac{\partial \Phi}{\partial r}\right)_{r=R}\mathrm{d}x\,R\,\mathrm{d}\theta, \tag{17}$$

where the negative sign must be chosen for an internal flow (with respect to the shell) and the positive sign for an external flow. In fact, the global contribution to the energy of the integration of $\Phi\,(\partial\Phi/\partial r)$ over the two surfaces at $x = 0$ and L is zero. By using equation (9), equation (17) is transformed into the following expression:

$$E_F = \mp\frac{1}{2}\rho_F \int_0^{2\pi}\int_0^L (\Phi)_{r=R}\left(\frac{\partial w}{\partial t} + U\,\frac{\partial w}{\partial x}\right) \mathrm{d}x\, R\, \mathrm{d}\theta. \tag{18}$$

The energy E_F can conveniently be divided into three terms having different dependencies on the exponent Λ:

$$E_F = -\Lambda^2\, T_F^* + \Lambda E_G + V_F. \tag{19}$$

The reference kinetic energy T_F^* of the fluid associated with the perturbation potential, similarly to equation (26) in Part I, is given by

$$T_F^* = \pm\frac{1}{2}\rho_F\, R\,\frac{L}{2}\,\pi\left[2\sum_{m=1}^{\infty}\sum_{j=1}^{3} a_{0mj}^2\,\frac{F_{0m}(\mathrm{R})}{(m\pi/L)} + \sum_{n=1}^{\infty}\sum_{m=1}^{\infty}\sum_{j=1}^{3}(a_{nmj}^2 + b_{nmj}^2)\,\frac{F_{nm}(R)}{(m\pi/L)}\right]. \tag{20}$$

In equation (20), the negative sign must be taken for an external flow. The reference kinetic energy of the fluid associated with the mean flow is not included in the shell equations of motion; therefore, it is not considered here. The maximum potential energy V_F is

$$V_F = \mp\frac{1}{2}\rho_F\, R\,\frac{L}{2}\,\pi U^2\left[2\sum_{m=1}^{\infty}\sum_{j=1}^{3} a_{0mj}^2\,(m\pi/L)\,F_{0m}(R) + \sum_{n=1}^{\infty}\sum_{m=1}^{\infty}\sum_{j=1}^{3}(a_{nmj}^2 + b_{nmj}^2)\,(m\pi/L)\,F_{nm}(R)\right], \tag{21}$$

where the negative sign is associated with an internal flow. Equation (21) shows that V_F is negative for both internal and external flows, i.e., the stiffness of the system decreases with U. This explains the shell instability at high flow velocities.

The maximum gyroscopic energy E_G associated with the perturbation potential is

$$\begin{aligned} E_G = \mp\frac{1}{2}\rho_F\, R\,\pi U\Bigg\{ & 2\sum_{m,i=1}^{\infty}\sum_{j,\tilde{j}=1}^{3} a_{0mj}\,a_{0i\tilde{j}}\int_0^L [(m/i)\,F_{0i}(R)\sin(i\pi x/L)\cos(m\pi x/L) \\ & + F_{0m}(R)\sin(i\pi x/L)\cos(m\pi x/L)]\,\mathrm{d}x \\ & + \sum_{n=1}^{\infty}\sum_{m,i=1}^{\infty}\sum_{j,\tilde{j}=1}^{3}(a_{nmj} + b_{nmj})\,(a_{ni\tilde{j}} + b_{ni\tilde{j}})\int_0^L [(m/i)\,F_{ni}(R)\sin(i\pi x/L)\cos(m\pi x/L) \\ & + F_{nm}(R)\sin(i\pi x/L)\cos(m\pi x/L)]\,\mathrm{d}x\Bigg\}, \end{aligned} \tag{22}$$

where the negative sign is associated to an internal flow. Equation (22) can easily be transformed into

$$\begin{aligned} E_G = \mp\frac{1}{2}\rho_F R\pi U\Bigg\{ & 2\sum_{m,i=1}^{\infty}\sum_{j,\tilde{j}=1}^{3} a_{0mj}\,a_{0i\tilde{j}}\,\alpha_{im}[(m/i)\,F_{0i}(R) + F_{0m}(R)] \\ & + \sum_{n=1}^{\infty}\sum_{m,i=1}^{\infty}\sum_{j,\tilde{j}=1}^{3}(a_{nmj} + b_{nmj})\,(a_{ni\tilde{j}} + b_{ni\tilde{j}})\,\alpha_{im}[(m/i)\,F_{ni}(R) + F_{nm}(R)]\Bigg\}, \end{aligned} \tag{23}$$

where

$$\alpha_{im} = \int_0^L \sin(i\pi x/L)\cos(m\pi x/L)\,\mathrm{d}x$$

$$= \left\{ \begin{array}{ll} 0 & \text{if } m = i, \\ 0 & \text{if both } m \text{ and } i \text{ are even or odd,} \\ \dfrac{L[-2i + (m+i)(-1)^{i-m} - (m-i)(-1)^{m+i}]}{2\pi(m-i)(m+i)} & \text{otherwise.} \end{array} \right\}.$$

One can immediately verify that E_G is globally zero as a consequence of the fact that $(m/i)\alpha_{im} = -\alpha_{mi}$. This proves that the system is conservative and that no energy is dissipated. It is to be noted that equation (23) expresses a coupling between modes that is characteristic of gyroscopic systems. Thus, equation (23) will be used in Section 5 to evaluate the gyroscopic matrix **C**.

3. EFFECT OF THE PRESSURE AND THE INITIAL PRE-STRESS

The substitution of the mode expansion, equation (7), into the operator obtained by using the Flügge theory of shells (Leissa 1973) gives the following matrix:

$$\mathbf{L}_F = \begin{bmatrix} -\lambda^2 - (1+k)\dfrac{1-v}{2}n^2 + \Omega^2 & \pm\dfrac{1+v}{2}\lambda n & v\lambda - k\lambda\left(\lambda^2 + \dfrac{1-v}{2}n^2\right) \\ \pm\dfrac{1+v}{2}\lambda n & -\dfrac{1-v}{2}\lambda^2(1+3k) - n^2 + \Omega^2 & \mp n \mp \dfrac{3-v}{2}k\lambda^2 n \\ -v\lambda + k\lambda\left(\lambda^2 + \dfrac{1-v}{2}n^2\right) & \pm n \pm \dfrac{3-v}{2}k\lambda^2 n & 1 + k(\lambda^2+n^2)^2 + k(1-2n^2) - \Omega \end{bmatrix}, \tag{24}$$

where $\lambda = m\pi R/L$, and there are two different signs for some elements; the sign above is chosen for symmetric modes with respect to $\theta = 0$ and the one below for antisymmetric modes. The additional matrix, according to the Flügge theory for taking into account initial pre-stress of the shell is (Leissa 1973)

$$\mathbf{L}_P = \frac{1}{c}\begin{bmatrix} -n^2N_\theta - \lambda^2 N_x \pm 2\lambda n N_{x\theta} & 0 & -\lambda N_\theta \\ 0 & -n^2N_\theta - \lambda^2 N_x \pm 2\lambda n N_{x\theta} & \mp nN_\theta + 2\lambda N_{x\theta} \\ \lambda N_\theta & \pm nN_\theta + 2\lambda N_{x\theta} & n^2N_\theta + \lambda^2 N_x \pm 2\lambda n N_{x\theta} \end{bmatrix}, \tag{25}$$

where $c = Eh/(1 - v^2)$; N_x, N_θ and $N_{x\theta}$ are the membrane uniform forces per unit length, in the axial, circumferential and tangential directions, respectively. These membrane forces can have different physical origins. In the case of a uniform radial pressure $\bar{P}$, assumed positive outwards, the circumferential force per unit length is $N_\theta = R\bar{P}$ and $N_x = 0$ for a simply supported shell. For shells axially constrained, $N_x \neq 0$ in the case of a uniform radial pressure; in particular, $N_x = vR\bar{P}$ for $u = 0$ at $x = 0, L$. The case of axial elastic constraints is investigated in Appendix B.

In the case of a viscous flow, the steady viscous effect gives an almost constant axial force per unit area p_x; this gives a membrane force per unit length $N_x = p_x(\frac{1}{2}L - x)$. This linearly varying membrane force cannot be studied with equation (25) but requires a different operator; this problem will be investigated in Part III of the present study.

The frequency equation of the shell with pre-stress is obtained by

$$\det[\mathbf{L}_F + \mathbf{L}_P] = 0, \tag{26}$$

which has three roots Ω_{nmj} for any given values of n and m; these roots, corresponding to $j = 1, 2, 3$, have modes with prevalent radial, longitudinal and circumferential displacements, respectively. These values are the same for symmetric and antisymmetric modes with respect to $\theta = 0$. In equation (24), Ω_{nmj} is the frequency parameter, defined by

$$\Omega_{nmj}^2 = \omega_{nmj}^2 R^2 \rho_S (1 - v^2)/E, \tag{27}$$

where ω_{nmj} is the corresponding circular frequency, ρ_S is the shell mass density, E is Young's modulus, and v is the Poisson ratio. The mode shape coefficients A_{nmj} and B_{nmj} are obtained as eigenvectors of equation (26), after normalization to one of the third element of each eigenvector. Only a change in sign is found in the mode shape coefficients of symmetric and antisymmetric modes.

4. NONSYMMETRIC CONSTRAINTS

The elastic constraints at the shell edges have been considered in Part I of the present study. In this section, the extension to the case of different constraints at $x = 0$ and L is considered. The maximum potential energy $V_{\tilde{k}}$ stored by the elastic distributed springs, which simulate the flexible axial translational constraint at $x = 0, L$, is given by

$$V_{\tilde{k}} = \frac{1}{2}\int_0^{2\pi} \tilde{k}_0(\theta)\, u^2(0, \theta)\, R\, \mathrm{d}\theta + \frac{1}{2}\int_0^{2\pi} \tilde{k}_L(\theta)\, u^2(L, \theta)\, R\, \mathrm{d}\theta. \tag{28}$$

In equation (28), $\tilde{k}_0(\theta)$ and $\tilde{k}_L(\theta)$ are the nonuniform spring stiffnesses ($\mathrm{N/m^2}$) at $x = 0$ and L, respectively. For simplicity, $\tilde{k}_0(\theta)$ and $\tilde{k}_L(\theta)$ are assumed to be symmetric with respect to $\theta = 0$, and it can be expanded into the following cosine series:

$$\tilde{k}_x(\theta) = \sum_{k=0}^{\infty} \tilde{k}_{x,k} \cos(k\,\theta), \quad \text{where } x = 0, L. \tag{29}$$

For symmetric modes, substitution of equations (7) and (29) into equation (28) gives

$$V_{\tilde{k}} = \frac{1}{2} R \sum_{n,s=0}^{\infty} \sum_{m,i=1}^{\infty} \sum_{j,\,\tilde{j}=1}^{3} \sum_{k=0}^{\infty} \psi_{nsk}\, a_{nmj}\, a_{si\tilde{j}}\, A_{nmj}\, A_{si\tilde{j}} [\tilde{k}_{0,k} + \tilde{k}_{L,k}(-1)^m(-1)^i], \tag{30}$$

where ψ_{nsk} is defined in Part I. The extension for antisymmetric modes and rotational constraints is analogous.

5. EIGENVALUE PROBLEM

Only a finite number of modes in the Rayleigh–Ritz expansion is retained. The three-dimensional matrix $\mathbf{q}$ of the Ritz coefficients is introduced as

$$q_{nmj} = \begin{cases} a_{nmj} & \text{for symmetric modes, } n = 0, \ldots, N-1;\ m = 1, \ldots, \tilde{N},\ j = 1, 2, 3, \\ b_{nmj} & \text{for antisymmetric modes, } n = 1, \ldots, N;\ m = 1, \ldots, \tilde{N},\ j = 1, 2, 3. \end{cases} \tag{31}$$

In equation (31), the expansion of symmetric and antisymmetric modes involves $3 \times N \times \tilde{N}$ terms; N and $\tilde{N}$ must be chosen large enough to give the required accuracy.

The reference kinetic energy of the fluid associated with to the perturbation potential, equation (20), can be written as

$$T_F^* = \tfrac{1}{2}\,\rho_F\, R(L/2)\,\mathbf{q}^{\mathrm{T}}\,\mathbf{M}_F\,\mathbf{q}, \tag{32}$$

where the matrix $\mathbf{M}_F$ is given by

$$(\mathbf{M}_F)_{nsmij\tilde{j}} = \pm \begin{cases} 2\,\delta_{ns}\,\delta_{mi}\,\delta_{j\tilde{j}}\,\dfrac{F_{0m}(R)}{(m/L)} & \text{if } n = 0, \\ \delta_{ns}\delta_{mi}\delta_{j\tilde{j}}\,\dfrac{F_{nm}(R)}{(m/L)} & \text{if } n > 0. \end{cases} \tag{33}$$

The maximum potential energy of the fluid is

$$V_F = -\tfrac{1}{2}\,\rho_F\, R(L/2)\pi U^2\,\mathbf{q}^{\mathrm{T}}\,\mathbf{K}_F\,\mathbf{q}, \tag{34}$$

where the matrix $\mathbf{K}_F$ is given by

$$(\mathbf{K}_F)_{nsmij\tilde{j}} = \pm \begin{cases} 2\,\delta_{ns}\delta_{mi}\delta_{j\tilde{j}}(m\pi/L)F_{0m}(R) & \text{if } n = 0, \\ \delta_{ns}\,\delta_{mi}\,\delta_{j\tilde{j}}(m\pi/L)F_{nm}(R) & \text{if } n > 0. \end{cases} \tag{35}$$

The energy transferred among modes, associated with the gyroscopic effect, is

$$E_G = -\tfrac{1}{2}\,\rho_F\, R\pi U\mathbf{q}^{\mathrm{T}}\mathbf{C}_F\mathbf{q}, \tag{36}$$

where the matrix $\mathbf{C}_F$ is given by

$$(\mathbf{C}_F)_{nsmij\tilde{j}} = \pm \begin{cases} 2\delta_{ns}\,\alpha_{im}[(m/i)\,F_{0i}(R) + F_{0m}(R)] & \text{if } n = 0, \\ \delta_{ns}\,\alpha_{im}[(m/i)\,F_{ni}(R) + F_{nm}(R)] & \text{if } n > 0. \end{cases} \tag{37}$$

The stiffness matrices associated with the translational and rotational springs given in Part I can easily be modified to take into account different edge constraints, as discussed in Section 4. The effect of pressure and initial pre-stress is taken into account by the potential energy of the shell, as presented in Part I, inserting the natural circular frequency ω_{nmj}, obtained by equation (26). In equations (33), (35) and (37) the positive sign must be taken for an internal flow and the negative one for an external flow.

The equation of motion of the system can be written in the following vectorial form:

$$\mathbf{M}\ddot{\mathbf{x}} + \mathbf{C}\dot{\mathbf{x}} + \mathbf{K}\mathbf{x} = \mathbf{0}, \tag{38}$$

where

$$\mathbf{M} = \rho_S\, h(L/2)\,\mathbf{M}_S + \rho_F(L/2)\,\mathbf{M}_F + (M/R)\,\mathbf{M}_M, \tag{39}$$

$$\mathbf{K} = \rho_S\, h(L/2)\,\mathbf{K}_S - \rho_F(L/2)\pi U^2\,\mathbf{K}_F + \mathbf{K}_{\tilde{k}} + \mathbf{K}_c + \mathbf{K}_B, \tag{40}$$

$$\mathbf{C} = -\rho_F \pi U \mathbf{C}_F, \tag{41}$$

$$\mathbf{x}(t) = \mathrm{e}^{\Lambda t}\mathbf{q}. \tag{42}$$

Matrices $\mathbf{M}_S$, $\mathbf{M}_M$, $\mathbf{K}_S$, $\mathbf{K}_{\tilde{k}}$, $\mathbf{K}_c$ and $\mathbf{K}_B$ are defined in Part I. Equation (38) is solved in state space, and gives the following eigenvalue problem:

$$\Lambda \begin{Bmatrix} \mathbf{q} \\ \Lambda\mathbf{q} \end{Bmatrix} = \begin{bmatrix} \mathbf{0} & \mathbf{I} \\ -\mathbf{M}^{-1}\mathbf{K} & -\mathbf{M}^{-1}\mathbf{C} \end{bmatrix} \begin{Bmatrix} \mathbf{q} \\ \Lambda\mathbf{q} \end{Bmatrix}. \tag{43}$$

In equation (43), $\{\mathbf{q}, \Lambda\mathbf{q}\}^{\mathrm{T}}$ is the state vector. It must be observed that the eigenvalue Λ is generally complex. In the present case, it has been shown at the end of Section 2 that the system is conservative. Therefore, before the onset of instability, the eigenvalues have a zero real part. In general, eigenvectors $\mathbf{q}$ have both real and imaginary parts different from zero; therefore, modes are complex. The only exception is for zero flow velocity U.

6. NUMERICAL IMPLEMENTATION

The solution of the problem is obtained with a self-made code written in *C* language. The matrices with six indices given in Section 5 are transformed into matrices with two indices (plane matrices); this transformation is explained in Part I of the present study. A routine to find the complex eigenvalues and eigenvectors of the generic matrix has been used. In particular, it is a modified version of the *Eispack rg* "real general" routine.

7. NUMERICAL RESULTS

Numerical results are obtained for shells containing flowing water (i) to validate the method and the computer code; (ii) to investigate the effect of different boundary conditions at the shell ends, including the solution of the paradox of Horáček and Zolotarev (1984); (iii) to study riveted shells; (iv) to investigate the effect of the static pressure. Moreover, shells in external water flow and in annular air flow have also been analysed.

7.1. Validation of the Method

A study has been performed for a case already studied in the literature, in order to make comparisons. The case analysed here was studied analytically by (i) Weaver & Unny (1973) by considering rigid extensions to the shell being studied, (ii) Amabili *et al.* (1999) considering both rigid and flexible extensions and (iii) Selmane & Lakis (1997*a*) considering flexible extensions only. It is a circular cylindrical shell, simply supported at the ends, containing flowing water and having the following characteristics: $L/R = 2$, $h/R = 0{\cdot}01$, $E = 206 \times 10^9$ Pa, $\rho = 7850$ kg/m^3, $\rho_F = 1000$ kg/m^3 and $\nu = 0{\cdot}3$. A nondimensional fluid velocity V is introduced for convenience, defined as in Weaver & Unny (1973) by $V = U/\{(\pi^2/L)[D/(\rho h)]^{1/2}\}$, with $D = E h^3/[12(1-\nu^2)]$; similary, a nondimensional, generally complex, eigenfrequency Ω is defined as $\Omega = \Lambda/\{(\pi^2/L^2)[D/(\rho h)]^{1/2}\}$, Λ being the corresponding complex radian eigenfrequency.†

Figure 2 shows the imaginary and real parts of the nondimensional eigenvalues Ω versus the nondimensional flow velocity for modes having five circumferential waves ($n = 5$), including the fundamental mode ($n = 5$, $m = 1$ for $V = 0$). Results have been obtained by

†Strictly, Λ and hence Ω are eigenvalues, but are here referred to as eigenfrequencies.

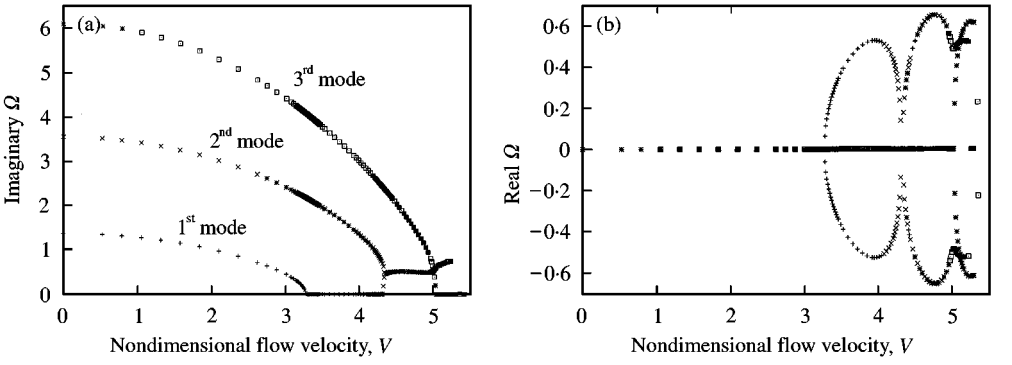

Figure 2. First three nondimensional eigenvalues Ω with $n = 5$ circumferential waves for the simply supported shell conveying water versus the nondimensional flow velocity. (a) Imaginary part of Ω (frequency); (b) real part of Ω (damping).

using nine longitudinal modes in the expansion although only the first three longitudinal modes are reported in Figure 2. It is to be noted that many of the results available in the literature have been obtained while retaining only two or three longitudinal modes in the expansion. These results are in good agreement with those reported by Amabili *et al.* (1999), for the case of flexible extensions that were obtained by using only two longitudinal modes; therefore, the agreement for the first mode is much better than that for the second mode. Results are close to those obtained for a shell with rigid extensions given in Amabili *et al.* (1999) and Weaver & Unny (1973), as already discussed by Amabili *et al.* (1999).

In Figure 2(a), the curves give the nondimensional frequency (imaginary part of Ω) of the shell versus the nondimensional fluid velocity V. Eigenfrequencies generally decrease with V. The lowest curve corresponds to the mode with one longitudinal wave ($m = 1$) for $V = 0$; the second curve to $m = 2$ and the third one to $m = 3$, for $V = 0$. The mode shape is changed by the flow, and the first mode can present two longitudinal waves for large flow velocities. Mode shapes at flow velocity $V = 1$ are shown in Figure 3. It is clear that the modes are complex; in particular, in Figure 3(a) the real part of the eigenvalue has a longitudinal half-wave (see shapes at $t = T/8$, $T/4$ and $3T/8$, where T is the time period) and the imaginary part has two longitudinal half-waves (see shape at $t = 0$ and $T/2$).

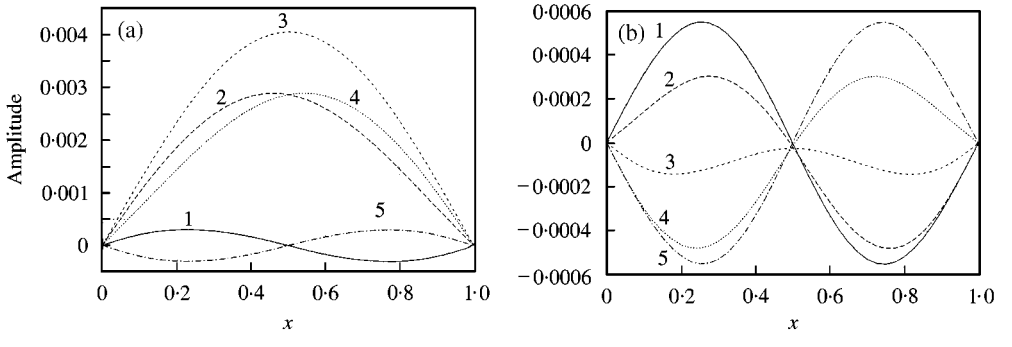

Figure 3. Radial mode shapes (in a radial section) with $n = 5$ circumferential waves for flow velocity $V = 1$ at five different instants $t = 0$ (1), $T/8$ (2), $T/4$ (3), $3T/8$ (4), $T/2$ (5), where T is the time period; simply supported shell. (a) First mode; (b) second mode.

Figure 2(b) gives the real part of the nondimensional eigenfrequency, proportional to damping; when $\mathscr{R}e(\Omega) > 0$, the system is unstable, whereas $\mathscr{R}e(\Omega) < 0$ indicates that the system is stable. The point where the lowest curve in Figure 2(a) reaches zero frequency, corresponds to the static divergence of the system ($V = 3{\cdot}33$). The intersection of the second curve with zero frequency gives the point of restabilization of the system ($V = 4{\cdot}34$). Then, the merging of the first- and second-mode loci corresponds to the onset of coupled-mode flutter, represented by the branch coming out from the curve corresponding to the second mode. It should be emphasized here that, strictly, the existence of coupled-mode flutter cannot be decided by a linear theory (it is a post-divergence behaviour of the shell involving large deformations) and was not predicted by Amabili *et al.* (1999) by using a nonlinear approach. In particular, that study has shown for the first time that the stability (divergence) limit predicted by using a linear theory can be largely nonconservative.

Figure 4 shows differences between data reported in Figure 2(a) and imaginary Ω (nondimensional frequency) computed with only three longitudinal modes in the expansion. The nondimensional eigenfrequency of the first mode is almost perfectly evaluated with three longitudinal modes in the expansion; small differences arise for the second mode. However, the frequency of the third mode cannot be accurately evaluated by using only three modes in the expansion, except for small flow velocities. In any case, the intersections of the curves with the abscissa axis are not changed by the number of longitudinal modes in the expansion.

Nondimensional eigenfrequencies of the first longitudinal mode for different numbers n of circumferential waves are given in Figure 5. It is clear that $n = 5$ is the fundamental mode for all the flow velocities before divergence of the shell.

7.2. Effect of the Boundary Conditions

The same shell investigated in Section 7.1 is analysed here for different boundary conditions at the shell ends. Figure 6 shows the imaginary and real parts of the eigenvalues Ω of a clamped shell at both $x = 0$, L versus the nondimensional flow velocity for modes with $n = 6$, including the fundamental mode ($n = 6$, $m = 1$ for $V = 0$). The results have been

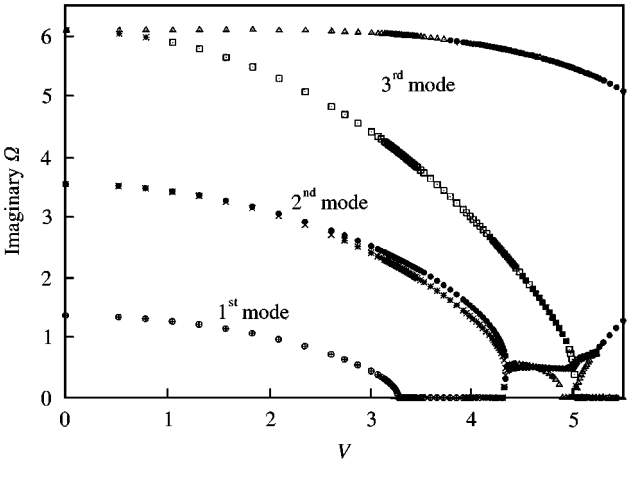

Figure 4. Comparison of the first three nondimensional eigenfrequencies evaluated with nine longitudinal modes (see Figure 2 where the same symbols are used) and three longitudinal modes (different symbols); $n = 5$, simply supported shell.

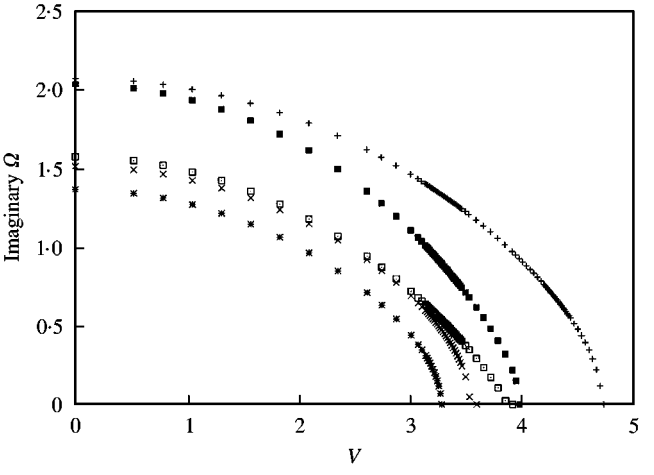

Figure 5. Nondimensional eigenfrequencies of the first longitudinal mode for different number n of circumferential waves versus the nondimensional flow velocity; simply supported shell conveying water: $*$, $n = 5$; $\times$, $n = 4$; $\boxdot$, $n = 6$; $\blacksquare$, $n = 7$; $+$, $n = 3$.

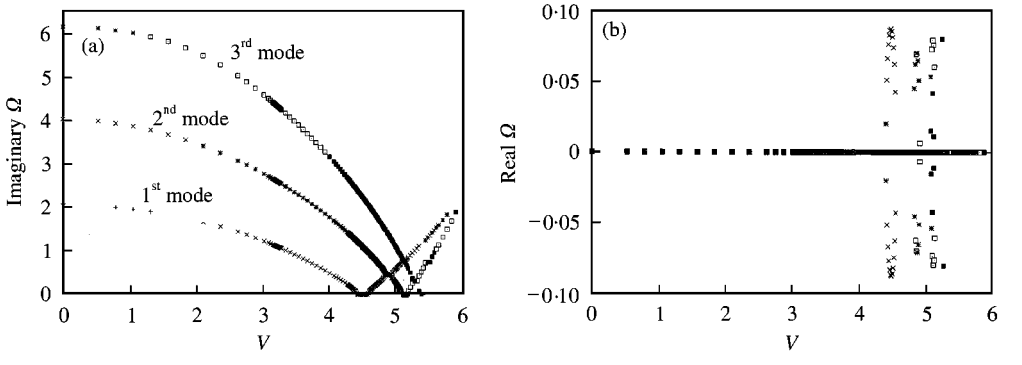

Figure 6. First three nondimensional eigenvalues Ω with $n = 6$ for clamped shell conveying water versus the nondimensional flow velocity. (a) Imaginary part of Ω (frequency); (b) real part of Ω (damping).

obtained by using nine longitudinal modes in the expansion. Figure 6(a) shows that nondimensional eigenfrequencies (imaginary Ω) are larger for the clamped shell with respect to the simply supported shell for any V, as expected. Eigenfrequencies of the first longitudinal mode for different values of n are given in Figure 7. Mode $n = 6$ is the fundamental mode for all the flow velocities before divergence of the shell, but has a frequency very close to the one of mode $n = 5$ for small flow velocity and to the one of mode $n = 4$ for large velocity. The crossing of curves corresponding to modes $n = 4$ and 5 is quite interesting.

Eigenvalues of the same shell clamped at the upstream end and simply supported downstream are shown in Figure 8, including the fundamental mode ($n = 5$, $m = 1$ for $V = 0$). Figure 8(b) shows that the system is conservative before the onset of instability (divergence), contradicting what was found by Horáček & Zolotarev (1984). The original result of Horáček & Zolotarev (1984) is probably due to some kind of numerical error in the eigenvalue evaluation. Eigenfrequencies and the critical velocity for this case are comprised between those of simply supported and those of clamped shells, as expected. Similarly,

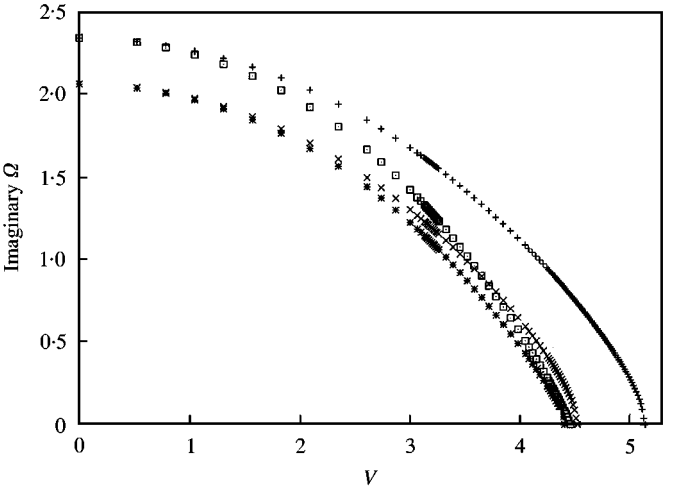

Figure 7. Nondimensional eigenfrequencies of the first longitudinal mode for different number n of circumferential waves versus the nondimensional flow velocity; clamped shell conveying water: $*$, $n = 6$; $\times$, $n = 5$; $\square$, $n = 4$; $+$, $n = 7$.

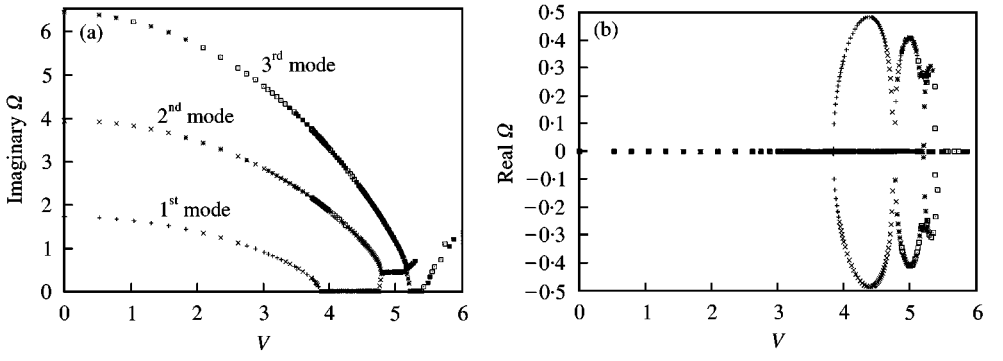

Figure 8. First three nondimensional eigenvalues Ω with $n = 5$ for clamped (upstream) – simply supported (downstream) shell conveying water versus the nondimensional flow velocity. (a) Imaginary part of Ω (frequency); (b) real part of Ω (damping).

Figure 9 gives the eigenvalues for the same shell simply supported at the upstream end and clamped downstream, i.e., with reversed boundary conditions; the results are almost coincident with those obtained in Figure 8.

7.3. Riveted Shells

The same shell investigated in Sections 7.1 and 7.2 is analysed here for nonuniform boundary conditions around the shell ends, as in the case of a riveted shell (see Part I of the present study). Figure 10 gives the nondimensional eigenfrequencies of symmetric and antisymmetric modes for a shell with four equispaced, almost clamped arcs, and simulating rivets, of angular amplitude of 3·6° at each shell end. These arcs are symmetrically distributed with respect to the origin ($\theta = 0$) and away from this point; both the slope in the axial direction and the axial displacements are restrained at the rivet location by using

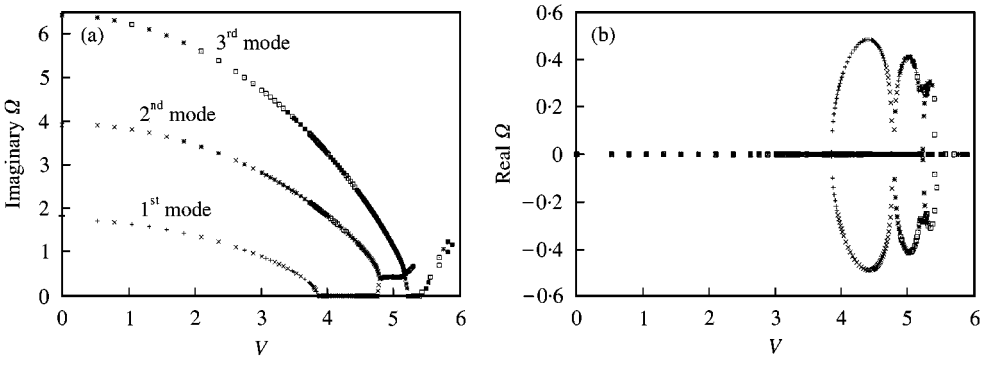

Figure 9. First three nondimensional eigenvalues Ω with $n = 5$ for simply supported (upstream) – clamped (downstream) shell conveying water versus the nondimensional flow velocity. (a) Imaginary part of Ω (frequency); (b) real part of Ω (damping).

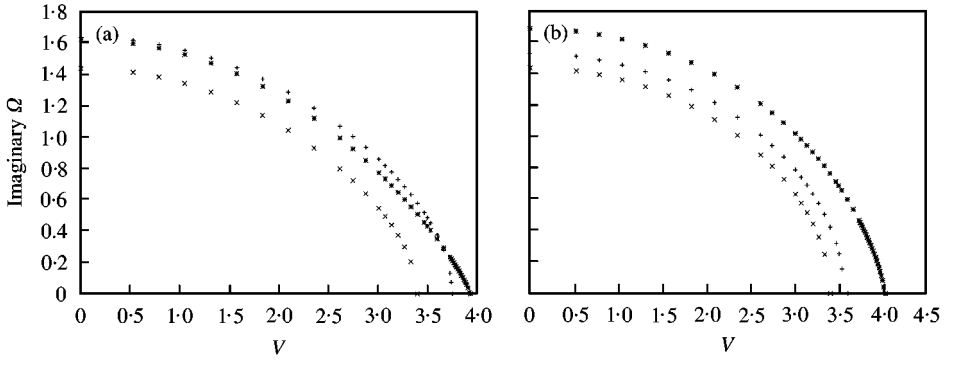

Figure 10. First three nondimensional frequencies for the shell with four rivets conveying water versus the nondimensional flow velocity. (a) Symmetric modes; (b) antisymmetric modes.

springs of very high translational stiffness $\tilde{k} = 10^9$ N/m^2 and rotational stiffness $c = 10^8$ N. Outside these clamped arcs the shell is simply supported. Results have been calculated by using an expansion with eight longitudinal and 19 circumferential modes (therefore the dimension of the vector of Ritz coefficients is $8 \times 19 \times 3$).

Complex mode shapes are shown in Figure 11 at a specific time instant ($t = T/4$, where T is the vibration period) for $V = 1$. Dots in Figure 11(a) indicate the location of rivets. The fundamental mode is the symmetric mode with five nodal diameters. It has a frequency slightly smaller than that of the first antisymmetric mode that also has five nodal diameters. The fundamental mode of the simply supported shell also has five nodal diameters, as shown in Figure 5. However, the third mode is antisymmetric with four nodal diameters, where the nodes are placed in correspondence to the clamped arcs. For this reason, this mode has only a very small change in frequency with respect to Figure 5.

Results for a shell containing flow with nonuniform boundary conditions around the edges have never been obtained before the present study.

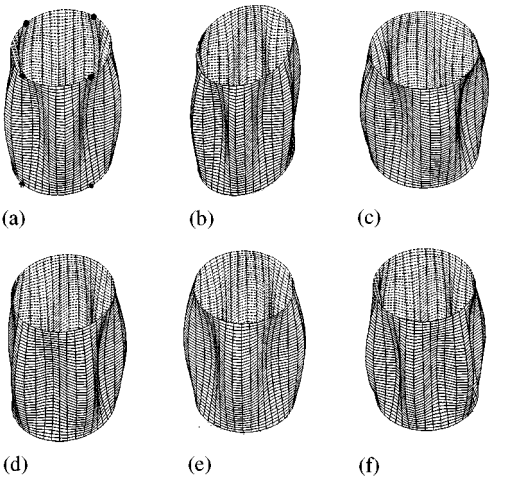

Figure 11. Radial mode shapes for flow velocity $V = 1$ at instant $t = T/8$, where T is the time period; shell with four rivets. (a) first symmetric mode, $\Omega = 1{\cdot}33$; dots indicate the location of rivets; (b) second symmetric mode, $\Omega = 1{\cdot}51$; (c) third symmetric mode, $\Omega = 1{\cdot}54$; (d) first antisymmetric mode, $\Omega = 1{\cdot}35$; (e) second antisymmetric mode, $\Omega = 1{\cdot}46$; (f) third antisymmetric mode, $\Omega = 1{\cdot}58$.

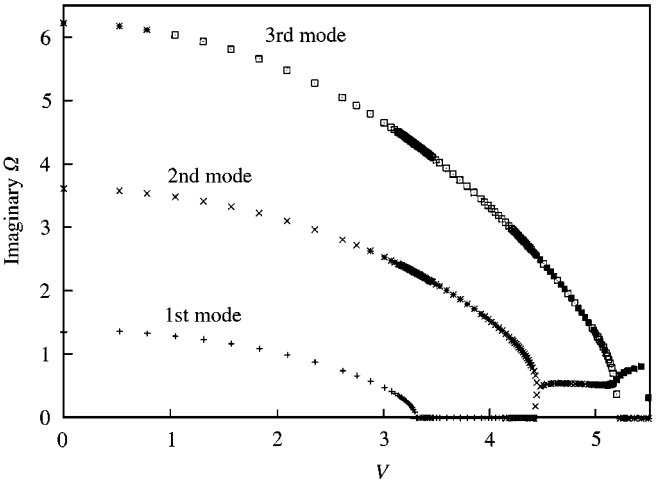

Figure 12. First three nondimensional eigenfrequencies with $n = 5$ for simply supported shell in axial unbounded water flow versus the nondimensional flow velocity.

7.4. Shell in an External Flow

The same shell studied in Section 7.1 is immersed in an unbounded axial flow of water. The shell is assumed to be simply supported at the ends. Figure 12 gives the nondimensional eigenfrequencies (imaginary part of Ω) versus the flow velocity; only small differences arise with respect to Figure 2(a). In fact, internal and external flows have almost the same effect on the shell considered; the effect of external water is only a little smaller than that of internal flow in this case.

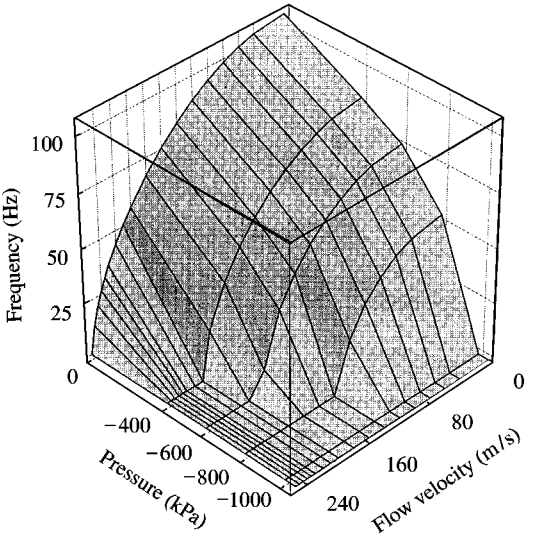

Figure 13. Eigenfrequency of the fundamental mode ($n = 5$) of the simply supported shell in axial unbounded water flow versus the static pressure and flow velocity; negative pressure is external.

7.5. Effect of Static Pressure

The effect of an external pressure on the frequency of the fundamental mode ($n = 5$, $m = 1$ for $V = 0$) of the simply supported shell with an external flow studied in Section 7.4 is shown in Figure 13. Here, dimensional data are given and the shell radius is assumed to be $R = 0{\cdot}5$ m. Variations of both pressure and flow velocity are analysed. The full range of possible pressures before shell buckling is considered. External pressure (negative value of $\bar{P}$) has the effect of decreasing the eigenfrequencies of the shell and of destabilizing it for all the range of flow velocities.

7.6. Shell in an Annular Flow

Numerical results were obtained for a case already theoretically and experimentally studied by El Chebair *et al.* (1989). It is a clamped–clamped circular cylindrical shell made of rubber, in annular incompressible air flow, having the following characteristics: $R = 0{\cdot}0247$ m, $L/R = 5{\cdot}5$, $h/R = 0{\cdot}05$, $R_1/R = 1{\cdot}25$, $E = 2{\cdot}43 \times 10^6$ Pa, $\rho = 1220$ kg/m^3, $\rho_F = 1{\cdot}25$ kg/m^3 and $\nu = 0{\cdot}47$. The static pressure inside and outside the shell was equal during the experiments, so that $\bar{P} = 0$ has been taken.

Eigenfrequencies of the first longitudinal mode for different values of n are given in Figure 14 versus the flow velocity (m/s). The fundamental mode is associated with $n = 2$ for all the flow velocity range. The second mode is associated with $n = 3$.

Eigenfrequencies of the first six longitudinal modes with $n = 3$, which is associated with the lowest flow velocity for instability according to experiments (where important nonlinear effects have been observed), are reported in Figure 15. When increasing the flow velocity, the mode shapes are changed from the classical ones of simply supported shells. As previously discussed, complex mode shapes arise. For small flow velocities, the real part of the mode, which has the same shape of the natural mode of the shell for zero flow, is predominant. For large flow velocities, the imaginary part, which usually has the shape of two longitudinal half-waves for the first mode, becomes predominant. In particular, for the first mode this

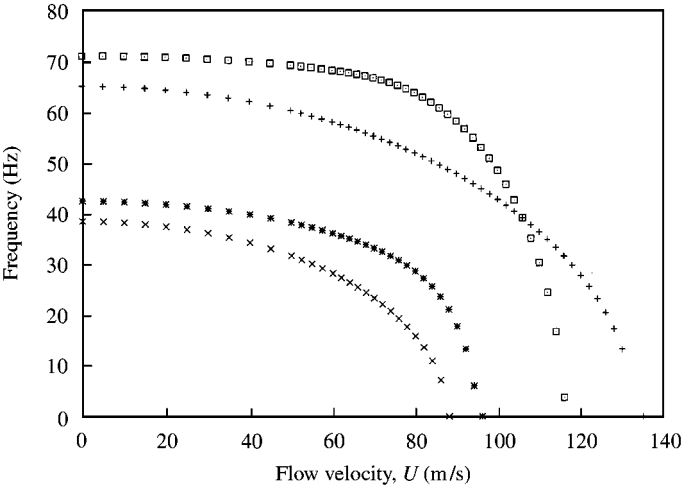

Figure 14. Eigenfrequencies of the first longitudinal modes for different number n of circumferential waves for clamped rubber shell in annular flow versus the air velocity: $\times$, $n = 2$; $*$, $n = 3$; $+$, $n = 1$; $\boxdot$, $n = 4$.

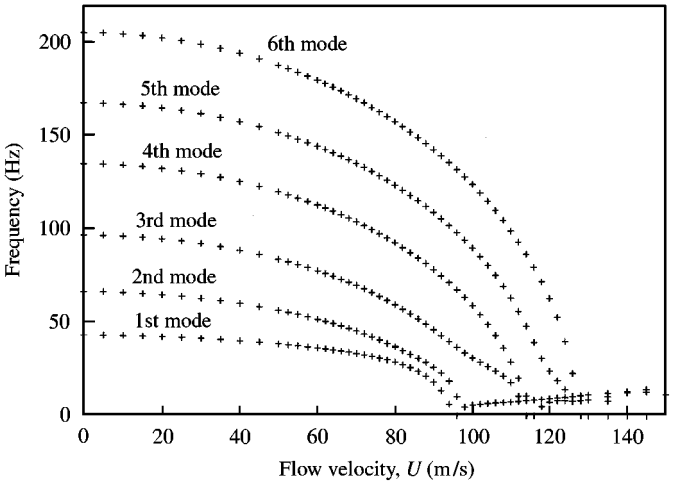

Figure 15. First six eigenfrequencies with $n = 3$ for clamped rubber shell in annular flow versus the air velocity.

change in shape arises for $U \simeq 60$ m/s. The system loses stability by divergence for a flow velocity around 80 m/s. Beyond this point, the system remains unstable; no restabilization is observed. The experimental results of El Chebair *et al.* (1989) are in good agreement with the linear, theoretical results at zero flow velocity. However, experiments show violent divergence at 49 m/s, i.e., *much before* the value predicted; moreover, the shape of the buckled shell at 49 m/s presents one axial half-wave ($n = 3$; $m = 1$), very large deformation and contraction of the circumference in a cross-section of the shell. Even if the effect of viscosity is included in the model (El Chebair *et al.* 1989), the theoretical predictions are significantly larger than the experimental results. In fact, as discussed by Amabili *et al.* (1999), the shell stability must be predicted by using a nonlinear theory to model shell dynamics; however, the eigenfrequencies can be predicted by using the present linear approach.

8. CONCLUSIONS

The present method has a large flexibility and allows the study of many complicating effects on the linear dynamics of shells with flowing fluid and nonuniform boundary conditions with a simple addition of an energy term associated with the single complication. This modularity of the method has given the possibility to develop the computer code DIVA, specifically dedicated to circular cylindrical shells. Internal, annular and external flows can be studied and the effects of static pressure, added masses, elastic bed and elastic constraints can be analysed.

Eigenfrequencies of shells coupled to an internal or an external flow generally decrease monotonically with the flow speed V. Initially, the frequency is very scarcely sensible to an increment of the flow speed; on approaching shell instability (divergence obtained for zero frequency) the frequencies decrease very rapidly by increasing V. Moreover, the vibration modes of the shell coupled to flow are complex. In particular, the fundamental mode has a real part having a predominant longitudinal half-wave, which is the natural mode for zero flow, and an imaginary part with predominant two half-wave terms. This complex mode is travelling along the shell length with the flow.

The study has also mathematically proved that shells with zero displacement at the shell ends and any additional internal or boundary constraint are conservative for any flow velocity before divergence of the system. The proof has been given for the fluid–structure interaction model obtained by separation of variables, corresponding to a flexible extension (of infinite length), periodically supported, of the shell. An extension of the method to shells with rigid baffles can easily be made.

ACKNOWLEDGMENTS

This research was partially supported by a grant of the Italian Space Agency (ASI).

REFERENCES

AMABILI, M. & GARZIERA, R. 2000 Vibrations of circular cylindrical shells with nonuniform constraints, elastic bed and added mass; Part I: empty and fluid-filled shells. *Journal of Fluids and Structures* **14,** 669–690.

AMABILI, M., PELLICANO, F. & PAÏDOUSSIS, M. P. 1999 Non-linear dynamics and stability of circular cylindrical shells containing flowing fluid. Part I: stability. *Journal of Sound and Vibration* **225,** 655–699.

AMABILI, M., PELLICANO, F. & PAÏDOUSSIS, M. P. 2000 Non-linear dynamics and stability of circular cylindrical shells containing flowing fluid. Part IV: large-amplitude vibrations with flow. *Journal of Sound and Vibration* **237,** 641–666.

DOWELL, E. H. & WIDNALL, S. E. 1966 Generalized aerodynamic forces on an oscillating cylindrical shell. *Quarterly of Applied Mathematics* **24,** 1–17.

EL CHEBAIR, A., MISRA, A. K. & PAÏDOUSSIS, M. P. 1990 Theoretical study of the effect of unsteady viscous forces on inner- and annular-flow-induced instabilities of cylindrical shells. *Journal of Sound and Vibration* **138,** 457–478.

EL CHEBAIR, A., PAÏDOUSSIS, M. P. & MISRA, A. K. 1989 Experimental study of annular-flow-induced instabilities of cylindrical shells. *Journal of Fluids and Structures* **3,** 349–364.

HORÁČEK, J. 1993 Approximate theory of annular flow-induced instabilities of cylindrical shells. *Journal of Fluids and Structures* **7,** 123–135.

HORÁČEK, J. & ZOLOTAREV, I. 1984 Influence of fixing edges of a cylindrical shell with conveying fluid on its dynamic characteristics. *Soviet Applied Mechanics* **20,** 756–765.

HORÁČEK, J. & ZOLOTAREV, I. 1991 Acoustic-structural coupling of vibrating cylindrical shells with flowing fluid. *Journal of Fluids and Structures* **5,** 487–501.

LEISSA, A. W. 1973 *Vibration of Shells*, NASA SP-288. Washington, DC: Government Printing Office. Now available from The Acoustical Society of America (1993).

MATSUZAKI, Y. & FUNG, Y. C. 1977 Unsteady fluid dynamic forces on a simply-supported circular cylinder of finite length conveying a flow, with applications to stability analysis. *Journal of Sound and Vibration* **54,** 317–330.

MISRA, A. K., WONG, S. S. T. & PAÏDOUSSIS, M. P. 2001 Dynamics and stability of pinned-clamped and clamped-pinned cylindrical shells conveying fluid. *Journal of Fluids and Structures* **15,** 1153–1166.

MIZOGUCHI, K. & KOMORI, S. 1978 Vibration and dynamic instability of a cylindrical shell conveying a compressible fluid. *Bulletin of the Japan Society of Mechanical Engineers* **21,** 628–636.

NIORDSON, F. I. N. 1953 Vibrations of cylindrical tube containing flowing fluid. Transactions of the Royal Institute of Technology, Stockholm, Sweden, No. 73.

NGUYEN, V. B., PAÏDOUSSIS, M. P. & MISRA, A. K. 1993 An experimental study of the stability of cantilevered coaxial cylindrical shells conveying fluid. *Journal of Fluids and Structures* **7,** 913–930.

NGUYEN, V. B., PAÏDOUSSIS, M. P. & MISRA, A. K. 1994 A CFD-based model for the study of the stability of cantilevered coaxial cylindrical shells conveying viscous fluid. *Journal of Sound and Vibration* **176,** 105–125.

PAÏDOUSSIS, M. P., CHAN, S. P. & MISRA, A. K. 1984 Dynamics and stability of coaxial cylindrical shells containing flowing fluid. *Journal of Sound and Vibration* **97,** 201–235.

PAÏDOUSSIS, M. P. & DENISE, J.-P. 1972 Flutter of thin cylindrical shells conveying fluid. *Journal of Sound and Vibration* **20,** 9–26.

PAÏDOUSSIS, M. P., MISRA, A. K. & CHAN, S. P. 1985 Dynamics and stability of coaxial cylindrical shells conveying viscous fluid. *Journal of Applied Mechanics* **52,** 389–396.

PAÏDOUSSIS, M. P., MISRA, A. K. & NGUYEN, V. B. 1992 Internal- and annular-flow-induced instabilities of a clamped–clamped or cantilevered cylindrical shell in a coaxial conduit: the effects of system parameters. *Journal of Sound and Vibration* **159,** 193–205.

PAÏDOUSSIS, M. P., NGUYEN, V. B. & MISRA, A. K. 1991 A theoretical study of stability of cantilevered coaxial cylindrical shells conveying fluid. *Journal of Fluids and Structures* **5,** 127–164.

SELMANE, A. & LAKIS, A. A. 1997*a* Vibration analysis of anisotropic open cylindrical shells subjected to a flowing fluid. *Journal of Fluids and Structures* **11,** 111–134.

SELMANE, A. & LAKIS, A. A. 1997*b* Non-linear dynamic analysis of orthotropic open cylindrical shells subjected to a flowing fluid. *Journal of Sound and Vibration* **202,** 67–93.

WEAVER, D. S. & UNNY, T. E. 1973 On the dynamic stability of fluid-conveying pipes. *Journal of Applied Mechanics* **40,** 48–52.

WONG, S. S. T. 2000 The dynamics of shells conveying fluid, with pinned–clamped and clamped–pinned boundary conditions. M.Eng. Thesis, Department of Mechanical Engineering, McGill University, Montreal, QC, Canada.

APPENDIX A: CONTRIBUTION OF THE MEAN FLOW TO THE ENERGY OF THE FLOW

When the mean flow is considered in the evaluation of the total flow energy, the following equation must be considered:

$$E_{TF} = \mp \frac{1}{2} \rho_F \int_{\Omega} (\Psi \partial \Psi / \partial n)|_{\Omega} \, \mathrm{d}\Omega, \tag{A1}$$

where Ω is the boundary surface of the fluid volume of length L, delimited by the shell surface and n is a coordinate along the normal to the boundary, taken positive outwards. For simplicity, let us consider the case of internal flow. The cases of annular and external flow can be studied similarly. In this appendix, it will be proved that equation (A1) can be reduced to equation (17) plus a constant term in time, which gives no contribution to the Rayleigh quotient and natural frequencies of the shell. Equation (A1) for internal flow, integrated over the shell internal surface and on the circular surfaces at $x = 0$, L gives

$$E_{TF} = -\frac{1}{2} \rho_F \int_0^{2\pi} \int_0^L (\Psi \partial \Psi / \partial r)\Big|_{r=R} \mathrm{d}x \, R \, \mathrm{d}\theta - \frac{1}{2} \rho_F \int_0^{2\pi} \int_0^R (\Psi \partial \Psi / \partial x)\Big|_{x=L} \mathrm{d}r r \, \mathrm{d}\theta$$

$$+\frac{1}{2}\rho_F \int_0^{2\pi}\int_0^R (\Psi\partial\Psi/\partial x)\Big|_{x=0} \mathrm{d}r r\,\mathrm{d}\theta. \tag{A2}$$

In equation (A2), $\partial\Psi/\partial r = \partial\Phi/\partial r$, $\partial\Psi/\partial x = U + \partial\Phi/\partial x$, $\Psi|_{x=L} = UL + \Phi$ and $\Psi|_{x=0} = \Phi$. Equation (A2) is therefore reduced to

$$E_{TF} = E_F - \frac{1}{2}\rho_F \int_0^{2\pi}\int_0^L (Ux\partial\Phi/\partial r)\Big|_{r=R} \mathrm{d}x\, R\,\mathrm{d}\theta - \frac{1}{2}\rho_F \int_0^{2\pi}\int_0^R UL(\partial\Phi/\partial x)\Big|_{x=L} \mathrm{d}r r\,\mathrm{d}\theta$$
$$-\frac{1}{2}\rho_F\, U^2\,\pi R^2\, L. \tag{A3}$$

The two integrals in equation (A3) give zero for $n \neq 0$ as a consequence of the fact that the result of integration between 0 and 2π of $\cos(n\theta)$ is zero (see equation (11) for the expression of Φ). For $n = 0$ it is necessary to substitute L by $2L$, which is the longitudinal period of motion, and the two integrals vanish. In fact, in Section 2.1, w was assumed to be a periodic function with main period $2L$ in order to obtain a separation of variables for Φ. As anticipated, the mean flow potential Ux gives no contribution to the evaluation of the flow energy, excluding a constant term, which does not affect the natural frequencies of the shell. In conclusion, the flow energy evaluated in Section 2.1 is completely justified.

APPENDIX B: AXIAL PRE-STRESS FOR PRESSURIZED SHELL WITH ELASTIC AXIAL CONSTRAINT

In the axial direction, the shell and the elastic constraints can be considered as three springs in series. The stiffness of the elastic constraint at $x = 0$ is

$$k_1 = \int_0^{2\pi} \tilde{k}_0(\theta)\, R\,\mathrm{d}\theta = 2\pi R\tilde{k}_{0,0}. \tag{B1}$$

Similarly, the stiffness of the elastic constraint at $x = L$ is

$$k_2 = \int_0^{2\pi} \tilde{k}_L(\theta)\, R\,\mathrm{d}\theta = 2\pi R\tilde{k}_{L,0}. \tag{B2}$$

The axial stiffness of the shell is

$$k_S = 2\pi\, RhE/L. \tag{B3}$$

The global stiffness of the system is

$$k_{eq} = 1\Big/\left(\frac{1}{k_1} + \frac{1}{k_S} + \frac{1}{k_2}\right). \tag{B4}$$

The membrane axial force per unit length is

$$N_x = (k_{eq}/k_S)\, vR\bar{P}. \tag{B5}$$

Equation (B5) gives a constant value for N_x; this value is exact in the case of uniform constraints around the edge, and it is an approximation, away form the edges, in the case of nonuniform constraints.